Manuscript ID: DOEBTO-UMD-9158-24-MM1

Full Citation: Menezes, M., Tancabel, J., Bacellar, D., & Aute, V. (2024). **Development & Experimental Validation of a Generalized Resistance-Capacitance Model for Numerical Simulation of Phase-Change Material Embedded Heat Exchangers**. *20th International Refrigeration and Air Conditioning Conference at Purdue*, July 15-18, 2024.

Development & Experimental Validation of a Generalized Resistance-Capacitance Model for Numerical Simulation of Phase-Change Material Embedded Heat Exchangers

Mylena MENEZES[1], James TANCABEL[2], Daniel BACELLAR[3], Vikrant AUTE[4]*

[1,2,3,4]Center for Environmental Energy Engineering
Department of Mechanical Engineering, University of Maryland
College Park, MD 20742 USA
Email: [1]mmenezes@umd.edu, [2]jmtanc@umd.edu, [3]dfbace@umd.edu, [4]vikrant@umd.edu

* Corresponding Author

ABSTRACT

Latent heat thermal energy storage (LHTES) using phase change material (PCM) has attracted increased attention as a viable solution for overcoming the mismatch between energy supply and demand for renewable energy-based systems. PCM-embedded heat exchangers (PCM-HX) have the potential to significantly improve thermal performance due to high storage capacity and low temperature variation during the phase change process. Most models for simulating LHTES heat transfer use Computational Fluid Dynamics (CFD) simulations, which have high computational costs resulting from considering the complex and time-dependent physics relevant to PCM-HXs. In this paper, a Generalized Resistance Capacitance-based Model (GRCM) was developed to predict the thermal performance of arbitrary PCM-HXs in a computationally efficient manner without compromising modeling accuracy. The GRCM is exercised for three case studies: (i) verification for a single-slabbed finned PCM-HX, (ii) verification and validation for a copper foam/paraffin composite PCM-HX, and (iii) validation for a straight tube annular finned PCM-HX. The copper foam PCM-HX uses an electric heater at the top of HX, while the other two configurations utilize water as heat transfer fluid. For the single-slabbed finned PCM-HX melting case, the mean deviation in average PCM temperature predicted by the GRCM compared to the CFD model was between 0.56 – 0.73 K, with maximum temperature deviation of 2.68 K. For the HTF outlet temperature, the validation results showed that GRCM prediction matches very well with experimental data, with mean temperature deviation of 0.24 K during melting case, while for solidification case was 0.34 K. These results showcase the GRCM's capability for accurately reproducing the thermal characteristics of PCM-HXs with considerably lower computational effort.

1. INTRODUCTION

The growing demand for more efficient renewable and sustainable technologies to mitigate implications of climate change has attracted significant research interest. Due to the intermittence of renewable energy-based systems, thermal energy storage (TES) arises as a solution to reduce the mismatch between energy supply and demand. Latent heat thermal energy storage (LHTES) using phase change material (PCM) is a great solution to store excess energy that would otherwise be wasted, thus decreasing energy fluctuations. One of the advantages of using PCM is their high latent heat of fusion and thermal stability, allowing them to store (and release) a large amount of thermal energy in a small temperature range (Piroozmand & Ahmadi, 2024).

However, the transient nature of PCM heat transfer requires computationally-expensive methods to predict charging and discharging process in PCM heat exchangers (PCM-HX). Most PCM-HX numerical models employ

Computational Fluid Dynamics (CFD), which can accurately predict complex, time-dependent physics, albeit at a high computational cost (Zhang et al., 2022). To this end, reduced-order models (ROMs) are often used to reliably predict PCM-HX performance in a computationally-efficient manner, allowing for testing different boundary conditions with minimal accuracy penalty (König-Haagen et al., 2023). For instance, Bacellar et al. (2021) proposed a reduced-order model using CFD results to develop a curve fit that correlates PCM temperature and mass fraction. The authors reported that the ROM showed excellent agreement with CFD simulations, with a 250,000x speed-up factor. In addition, Huang et al. (2022) proposed a black-box ROM that was verified against a finite-volume method (FVM) for a straight tube PCM-HX. Experimental data was used to train the black box model, which was 25 times faster than the FVM with only 3% accuracy penalty.

Resistance-Capacitance models (RCMs) have recently gained popularity for evaluating PCM-HX performance with acceptable computational cost. Compared to CFD, RCMs can accurately predict PCM-HX thermal-hydraulic performance with lower computational cost by assuming conduction as the main heat transfer mode, thus avoiding the need to solve for higher-order PCM-HX physics, e.g., natural convection during PCM melting. Neumann et al. (2021) developed an RCM for a plate heat exchanger where the outlet fluid and PCM temperature deviations compared to a finite-element model were 0.62 K and 0.85 K, respectively, with the benefit of a 20-30x computational reduction. An RCM for melting in periodic structure was developed and validated against experimental data by Alam et al. (2022), showing a mean temperature deviation range between 1.34 K to 2.81 K. The most important factor was the real-time factor (RTF) of the solver, which was on the order of 10^{-4}.

However, previous work with PCM-HX RCMs required creating a new resistance-capacitance network for every heat exchanger case of interest, which limits the ability to evaluate multiple PCM-HX geometries cost-effectively. To this end, we propose a computationally-efficient generalized RCM (GRCM) for predicting the thermal-hydraulic performance of PCM-HX. The GRCM is exercised for three case studies: (i) verification using literature data for a a single-slabbed finned PCM-HX (ii) verification and validation of a copper foam/paraffin HX and (iii) validation using in-house data for an annular finned HX. The PCM average temperature prediction during melting case for the a single-slabbed finned HX is verified against CFD simulation (Jalilian et al., 2024). For the copper foam/paraffin HX, the PCM temperature profile is verified against CFD model proposed by Alam (2023) and validated using experimental data from Zheng et al. (2018). Finally, the average PCM temperature profile and water outlet temperature for the annular finned HX are validated against in-house experimental data.

2. MODEL DESCRIPTION

2.1 Generalized Resistance-Capacitance Model (GRCM)

The GRCM is a computationally-efficient model capable of providing a good estimation of PCM transient behavior for any arbitrary Resistance-Capacitance network, unlike previous RCMs where a specific solver algorithm is required for every geometry. The geometry independence of GRCM provides flexibility to the solver, allowing rapid simulation by simultaneously solving the entire PCM-HX domain using a matrix inversion. The differences between the GRCM and RCM approaches are summarized in Table 1.

Table 1: Comparison of RCM and GRCM features

	RCM	**GRCM**
Solver	Geometry dependent	Geometry independent
Spatial marching	In series	Simultaneous (matrix inversion)
Computational cost	Low	Low
Flexible	No	Yes

Figure 1 shows the thermal networks for the RCM and GRCM. In the GRCM, the Resistance-Capacitance network is generated independently of heat exchanger geometry, while in the RCM is always uniform and geometry-dependent. The GRCM discretizes the PCM domain and calculates capacitances for each node. Resistances are placed based on horizontal and vertical connections as an array of pairs of nodes for each segment. The solver then calculates temperature difference using a simultaneous matrix inversion at each segment. Thereafter, the solver determines the temperature in the next time step and updates the flow time. The assumptions in the GRCM model include:

- Natural convection effects are disregarded, and conduction is the dominant heat transfer mode;

- No mass transfer across segments;
- The contact resistance between PCM and metal was neglected;
- Constant PCM thermophysical properties.

The domain is discretized into segments, where thermal resistances and capacitance of each segment are dependent upon the porosity. Segments with only metal structures have a porosity of 0, while segments with only PCM have a porosity value of 1. Segments containing both metal and PCM have volume-averaged porosity and thermophysical properties, as demonstrated by Alam et al. (2022).

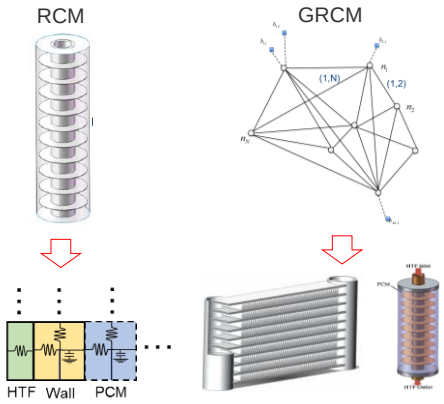

Figure 1: Resistance-Capacitance (RC) networks: (Left) RCM; (Right) GRCM

Capacitances are calculated based on volume of each segment and PCM thermophysical properties, as in Equations (1) and (2).

$$C = [\gamma_{PCM} C_{PCM} \rho_{PCM} + (1-\gamma_{PCM}) C_{metal} \rho_{metal}] V_{node} \tag{1}$$

$$C_{PCM} = \begin{cases} c_{p,\,sol} & T \le T_{sol} \\ c_{p,\,sol} + \dfrac{h_s}{T_{melt} - T_{sol}} & T_{sol} < T < T_{melt} \\ c_{p,\,liq} & T \ge T_{melt} \end{cases} \tag{2}$$

The general matrix equations utilized by the GRCM are summarized in Equations (3) to (5). The matrix M is defined by vertical and horizontal internal resistances along segments, which are calculated based on thermal conductivity, segment area and length, as showed in Alam et al. (2022). The matrix B considers the heat transfer at the PCM-HX boundaries using the wall temperature (T_{wall}) and boundary resistances ($R_{boundary}$) for all boundary segments, as showed in Equation (3). Then, the temperature change across the time step is calculated by taking the sum of all temperatures over the respective internal resistances summed by the heat transfer at the boundary, Equation (4). After calculating the temperature difference, the temperature for the next time step is updated based on Equation (5), where Δt is the time step.

$$B_i = \begin{pmatrix} \dfrac{T_{wall_i}}{R_{boundary_i}} \\ \vdots \\ \dfrac{T_{wall_i}}{R_{boundary_i}} \end{pmatrix} \tag{3}$$

$$\dot{T}_{i+1} = C_i^{-1}(MT_i + B_i) \tag{4}$$

$$T_{i+1} = T_i + \dot{T}_{i+1}\Delta t \tag{5}$$

The GRCM flowchart is demonstrated in Figure 2. The time marching is used to solve transient simulations for PCM storage devices. The solver initializes setting up capacitance, boundary and internal heat flow matrices. Then, GRCM calculates the temperature difference at each segment, solving a matrix inversion. Then, the solver updates the temperature at each segment for the next time step until the simulation time terminates.

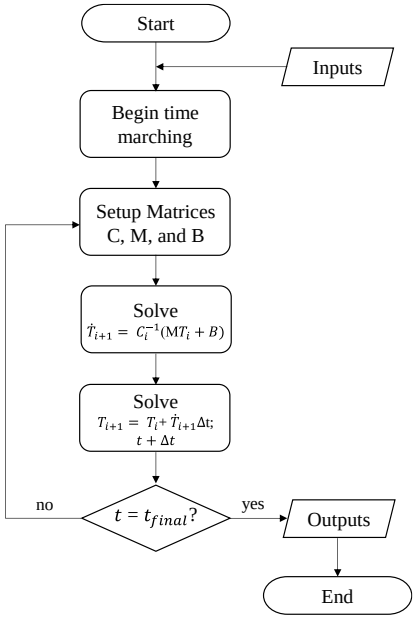

Figure 2: GRCM solution flowchart

3. PROBLEM DESCRIPTION

The aim of the study is to develop a numerical model that can accurately predict the thermal-hydraulic performance of PCM-HXs cost-effectively, regardless of the heat exchanger geometry. This study evaluates three different heat exchangers for GRCM verification and validation: (i) a single-slabbed finned PCM-HX (ii) PCM-HX embedded in copper foam and (iii) an annular finned PCM-HX.

3.1 Single-Slabbed Finned PCM-HX

Figure 3 shows the single finned-slab microchannel PCM-HX (Momeni et al., 2023). The PCM is located in the top section of the HX between fins, and hot water flows through 68 ports in the minichannel tube. The PCM-HX operating conditions are as follows: the water inlet temperature is 63 °C with a mass flow rate of 30 g/s, and the initial PCM temperature is 20°C. Aluminum is the material for the tube and fins. Three paraffin-based PCMs were considered: Docosane, Tetracosane, and Hexacosane, based on their availability, thermal properties, system compatibility, and practical application relevance (Jalilian et al., 2024). The detailed geometry of the single-slabbed finned PCM-HX is listed in Table 2. This PCM-HX analysis is accomplished assuming conjugate heat transfer at the bottom boundary condition, while the external boundaries are assumed adiabatic. To simulate the single-slabbed finned HX, a grid size of 170x11 (1870 elements) was selected, with total simulation time of 300 seconds and a time-step of 0.001 seconds.

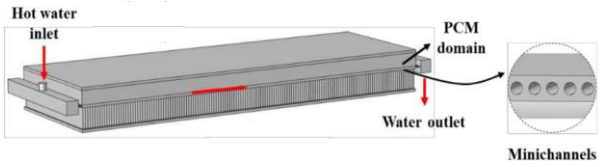

Figure 3: Single-slabbed finned PCM-HX domain and boundary conditions (Momeni et al., 2023)

Table 2: Single-slabbed finned PCM-HX geometry specifications (Momeni et al., 2023)

	Slab Width	Slab Length	Slab Height	Top Row Height	Number of fins	Fin Thickness	FPI	Channel Diameter	# of Tubes
Unit	mm	mm	mm	mm	-	mm	-	mm	-
Value	305	600	100	10.65	144	1.85	12	1	68

3.2 PCM-HX Embedded in Copper Foam

Figure 4 shows the PCM-HX using paraffin PCM embedded in copper foam, as proposed by Zheng et al. (2018). This heat exchanger was heated by an electrical heater attached on top of the PCM-HX, providing a constant heat flux of 1150 W/m^2. Three thermocouples were placed at 25, 50 and 100 mm from the heated wall (Figure 4b). The PCM-HX dimensions are 100x100x30 mm. To verify and validate the 3D geometry HX, a transient 2D GRCM model was used with a grid size of 20x20 (400 elements), total simulation time of 2150 s and a time-step of 0.5 seconds.

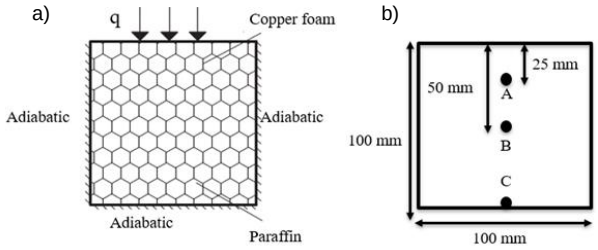

Figure 4: PCM-HX embedded in copper foam: (a) Domain and boundary conditions; (b) Thermocouple locations

3.3 Annular Finned HX

Figure 5a shows the annular finned PCM-HX which is representative of an optimum design proposed by Alam (2023). An in-house experimental study was conducted on a conventionally-manufactured PCM-HX prototype (Alam et al., 2024); this data was used to validate the GRCM. To simplify simulation and reduce computational cost, an axisymmetric domain was considered (Figure 5b). Figure 5c shows the thermocouple positions inside the PCM container used to measure PCM temperature in the experiment. Figure 5d demonstrates the RC-Network used for this heat exchanger. For the annular finned HX, a grid size of 260x8 (2080 elements) was chosen to compare with experimental data. The total simulation time is 360 and 250 seconds for melting and solidification cases, respectively, with a time-step of 0.005 seconds. The geometry specifications are provided in Table 3.

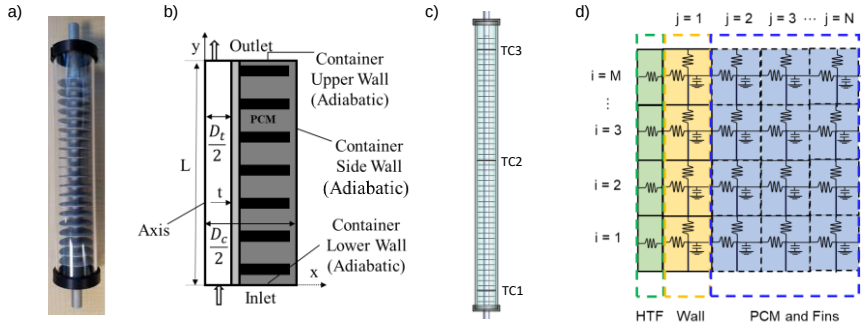

Figure 5: (a) Annular finned PCM-HX prototype; (b) Axisymmetric computational domain; (c) Thermocouple positions; (d) RC-Network

Table 3: Annular Finned PCM-HX geometry specifications

Tube Diameter (OD)	Tube Wall Thickness	Tube Length	Container Diameter (OD)	Container Wall Thickness	Number of fins	Fin Pitch	Fin Thickness	Fin Diameter
mm	mm	mm	mm	mm	-	mm	mm	mm
9.53	1.78	475.2	38.1	6.35	52	8.67	0.25	27.75

The thermophysical properties of all PCMs used in this work are given in Table 4. Docosane, Tetracosane and Hexacosane were the PCMs used in the single-slabbed finned PCM-HX (Jian-you, 2008; Kahwaji et al., 2018; Madruga et al., 2018). RT55 (Rubitherm GmbH, 2024a) was used for the PCM-HX embedded in copper foam, while RT62HC (Rubitherm GmbH, 2024b) was used in the annular finned PCM-HX.

Table 4: PCM thermophysical properties

PCM Properties	Docosane	Tetracosane	Hexacosane	RT55	RT62HC
k_{solid} (W/m-K)	0.37	0.37	0.22	0.20	0.20
k_{liquid} (W/m-K)	0.24	0.20	0.15	0.20	0.20
cp_{solid} (kJ/kg-K)	1.70	1.80	1.69	2.00	2.00
cp_{liquid} (kJ/kg-K)	2.20	2.10	2.19	2.00	2.00
Latent Heat (kJ/kg)	234	259	256	170	230
Density (kg/m³)	820	779	758	880	850
Melting Temperature Range (°C)	42.9 – 44.1	48.1 – 50.6	55.3 – 56.3	51 – 57	62.0 – 63.0

4. RESULTS AND DISCUSSION

4.1 GRCM Verification: Single-Slabbed Finned PCM-HX

Figure 6 shows a comparison of the average PCM temperature predictions from CFD and the GRCM for the melting case for three PCMs: (i) Docosane, (ii) Tetracosane and (iii) Hexacosane. For the tetracosane and hexacosane cases, the highest temperature deviation comes from the estimation of temperature glide during PCMs charging case. It is possible to observe from Figure 6 that even with the assumption of neglecting the effects of natural convection in the model, the GRCM demonstrated excellent agreement in predicting average PCM temperature compared to CFD simulation.

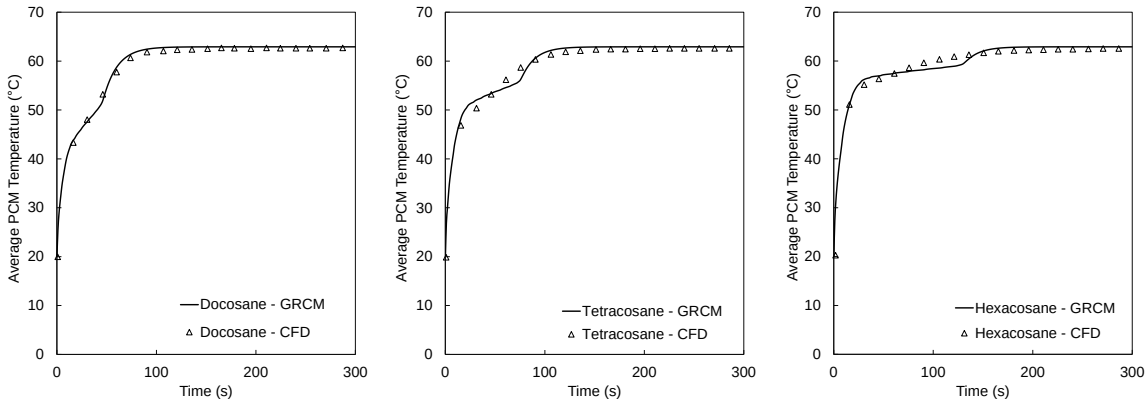

Figure 6: CFD vs. GRCM average PCM temperature: (Left) Docosane; (Center) Tetracosane; (Right) Hexacosane

Table 5 shows the accuracy prediction of GRCM compared to CFD. Compared to CFD simulation, the absolute mean deviation ranges from 0.6 – 0.7 K. This table also reports the maximum temperature deviation, which is 2.7 K for the tetracosane. The overall good agreement between GRCM and CFD showcases the ability of the GRCM to simulate different PCM-HX architectures with a high degree of accuracy and significantly less computational effort, e.g., the CFD grid used approximately 10^6 elements, while the GRCM used approximately 10^3 elements.

Table 5: Average PCM temperature deviation: CFD vs. GRCM

PCM	Absolute Mean Deviation (K)	Absolute Maximum Deviation (K)
Docosane	0.6	2.3
Tetracosane	0.7	2.7

Hexacosane	0.7	2.0

4.2 GRCM Verification & Validation: PCM-HX embedded with copper foam

The GRCM was verified and validated using CFD results proposed by Alam (2023), and experimental data for a PCM-HX embedded in copper foam proposed by Zheng et al. (2018). The left side of Figure 7 shows an excellent agreement of the average PCM temperature with both CFD and GRCM simulations, resulting in maximum temperature deviation of 0.29 K.

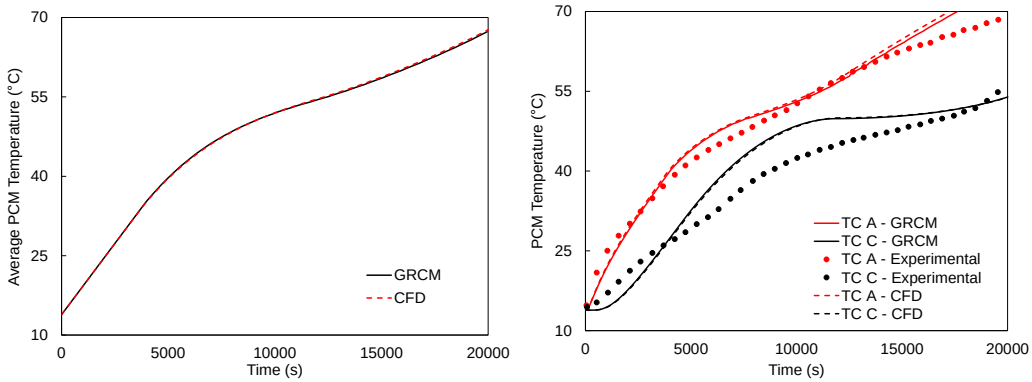

Figure 7: (Left) Average PCM temperature comparison between GRCM and CFD (Alam, 2023); (Right) PCM temperature profile at Thermocouple A and C: GRCM vs. experimental data (Zheng et al., 2018)

The right side of Figure 7 shows the PCM temperature profile at Thermocouple A (TC-A) and C (TC-C) for GRCM and CFD compared to the experimental data of Zheng et al. (2018). The deviation in temperature profile for TC-C is higher than for TC-A. It is worth to point out that TC-C is located at the bottom wall of the HX, opposite side of the heater, which was considered adiabatic during simulation. However, heat loss to the ambient during the experiment is unavoidable, which would result in higher GRCM-predicted temperatures compared to the experimental results. Comparing GRCM with experimental data, the mean temperature deviation for Thermocouples A and C are 1.57 K and 3.31 K, respectfully.

4.3 GRCM Validation of Annular Finned PCM-HX

GRCM validation was conducted for the annular finned PCM-HX utilizing in-house experimental data (Alam et al., 2024). Virtual thermocouples were placed in the same position as the experimental setup to compare the HTF outlet temperature and PCM temperature profiles during PCM melting and solidification. The experimental PCM average temperature was calculated by taking the average temperature of the thermocouple temperatures. Figure 8 shows the average PCM temperature comparison for GRCM and experimental data during melting and solidification. It is clear that the PCM temperature is overpredicted by the GRCM, which is likely due to neglecting heat loss to the ambient, and is more prominent during the melting case. Furthermore, during the PCM melting case, Thermocouple 3 (near the top) was exposed to air due to PCM thermal expansion during the phase-change process. Therefore, the measured temperature at this thermocouple location should be ignored. Nevertheless, the overall agreement is acceptable; the mean deviation between average PCM temperature for the GRCM and experimental data is 1.71 K.

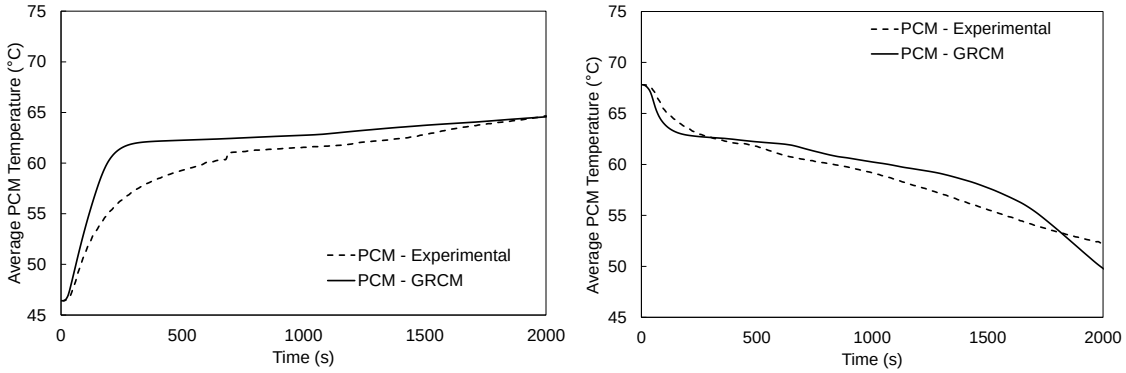

Figure 8: GRCM vs. experimental PCM average temperature:(Left) PCM melting; (Right) PCM solidification

For the solidification case, the maximum temperature deviation is 2.45 K, with mean deviation of 1.17 K. The temperature deviation can be explained by the overprediction of PCM phase-change and neglection of heat loss to the ambient, observed by taking the PCM temperature profile at each thermocouple, as shown in Figure 9. As can be seen, the GRCM starts with a good agreement for Thermocouples 1 and 3, then deviates from experimental data, delaying the phase change of PCM. This discrepancy in measurement could be explained by the phase change hysteresis (Klimeš et al., 2020), which is not accounted for in the GRCM simulation.

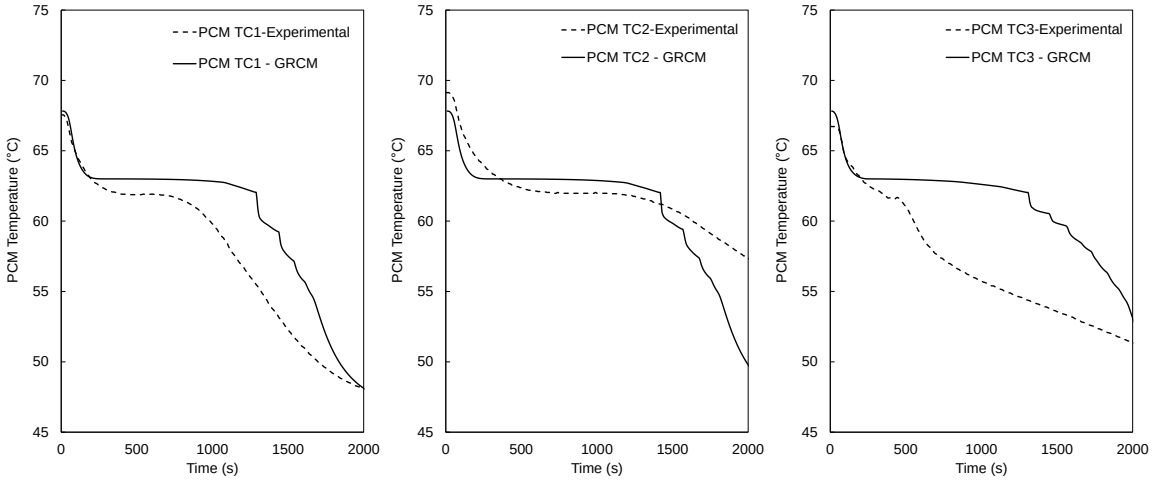

Figure 9: GRCM vs. experimental PCM temperature at each thermocouple position during PCM solidification

Figure 10 shows the comparison of experimental and predicted water outlet temperature for the melting and solidification cases. The predicted outlet water temperature matches very closely with experimental data. Overall, the deviation from experimental outlet water temperature increases over time, likely due to neglected heat loss. Compared to the experimental data, the mean temperature deviation during charging time is 0.24 K, while for the solidification case, the mean temperature deviation is 0.34 K, with maximum HTF outlet temperature deviation of 2.7 K.

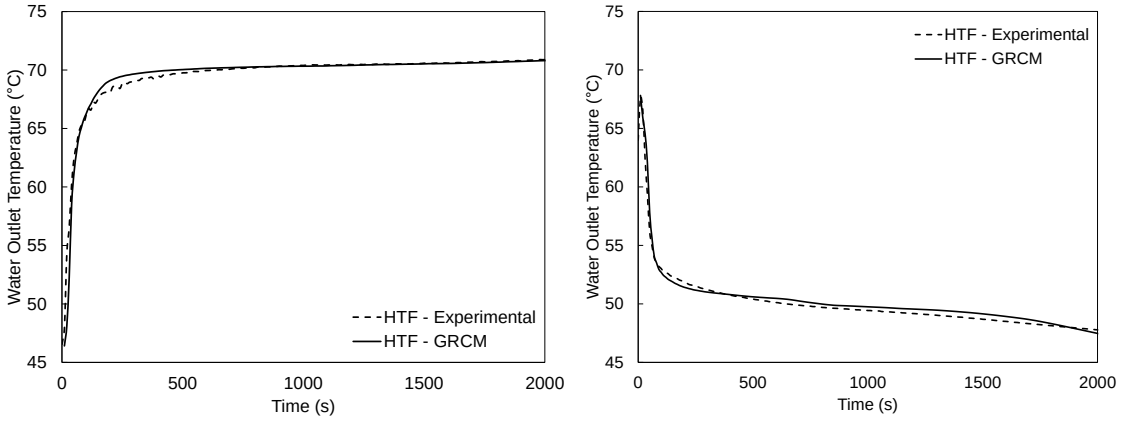

Figure 10: GRCM vs. experimental water outlet temperature; (Left) PCM melting; (Right) PCM solidification

5. CONCLUSIONS

Latent heat thermal energy storage using PCM is a key factor to increase renewable-energy based share in electricity production. One of the drawbacks of these systems is to determine the thermal-hydraulic performance with faster prediction and high accuracy. To decrease computational cost, a generalized resistance-capacitance model is proposed to accurately predict PCM storage devices. In this paper, GRCM was used for the verification and validation of three cases: (i) a single-slabbed finned PCM-HX, (ii) a copper foam/paraffin composite PCM-HX and (iii) a straight tube annular finned PCM-HX. The verification of single-slabbed finned HX with CFD simulation shows that the predicted PCM temperature profile over time agreement was between 0.56 – 0.73 K. The maximum PCM temperature deviation was 2.68 K for Tetracosane. For the verification and validation of copper foam/paraffin PCM-HX, the mean temperature deviation between GRCM and experimental data for Thermocouple A was 1.57 K, while for Thermocouple C was 3.31 K. The higher discrepancy in Thermocouple C was due to the assumption of adiabatic wall in the simulation, neglecting heat loss to the ambient. For the annular finned HX, the outlet water temperature prediction by GRCM shows a good agreement, with a mean temperature deviation of 0.24 K and 0.34 K for melting and solidification cases, respectively. These verifications and validations demonstrate that GRCM can efficiently and accurately predict PCM-HX thermal performance, opening new opportunities for design and optimization for novel, high-performance PCM-HXs for a wide variety of applications, such as domestic hot water heating, heat pump integrated with TES, heat management of photovoltaic thermoelectric systems, and so on.

NOMENCLATURE

B	Matrix of boundary heat flow	(W)	t	time	(s)
C	Thermal Capacitance	(J/kg-K)	V	Volume	(m^3)
c_p	Specific Heat	(J/kg-K)	γ	Porosity	(–)
h_s	Latent heat	(kJ/kg)	δ	Thickness	(mm)
M	Matrix of internal heat flow	(W)	Δ	Variation	(–)
R	Thermal Resistance	(K/W)	ρ	Density	(kg/m^3)
RCM	Resistance-Capacitance Model	(–)	**Subscript**		
ROM	Reduced-Order Model	(–)	i	index	(–)
RTF	Real-time Factor	(–)	liq	liquidous	(–)
T	Temperature	(K)	melt	melting	(–)
$\dot{T}$	Time Derivative of Temperature	(K/s)	sol	solidification	(–)

REFERENCES

Alam, T. (2023). *Development, Validation and Application of Resistance-Capacitance Based Models (RCM) for Phase Change Material Heat Exchangers* [University of Maryland]. https://doi.org/https://doi.org/10.13016/dspace/h1ku-eaj4

Alam, T., Bacellar, D., Ling, J., & Aute, V. (2022). Development and Validation of Resistance-Capacitance Model

for Phase Change Material Embedded in Porous Media. *InterSociety Conference on Thermal and Thermomechanical Phenomena in Electronic Systems, ITHERM*, *2022-May*(2011), 1–10. https://doi.org/10.1109/iTherm54085.2022.9899532

Alam, T., Yang, J., Bacellar, D., Tancabel, J., Muehlbauer, J., Hwang, Y., & Aute, V. (2024). Optimization and Experimental Validation of Annular Finned PCM-HX for a Domestic Hot Water Heater Application. *27th International Refrigeration and Air Conditioning Conference at Purdue*.

Bacellar, D., Alam, T., Ling, J., & Aute, V. (2021). A Study on Computational Cost Reduction of Simulations of Phase-Change Material (PCM) Embedded Heat Exchangers. *18th International Refrigeration and Air Conditioning Conference at Purdue*, 1–9.

Huang, R., Mahvi, A., Odukomaiya, W., Goyal, A., & Woods, J. (2022). Reduced-order modeling method for phase-change thermal energy storage heat exchangers. *Energy Conversion and Management*, *263*(April), 115692. https://doi.org/10.1016/j.enconman.2022.115692

Jalilian, S., Momeni, M., & Fartaj, A. (2024). Enhancing thermal performance and optimization strategies of PCM-integrated slab-finned two-fluid heat exchangers for sustainable thermal management. *Journal of Energy Storage*, *75*(August 2023), 109587. https://doi.org/10.1016/j.est.2023.109587

Jian-you, L. (2008). Numerical and experimental investigation for heat transfer in triplex concentric tube with phase change material for thermal energy storage. *Solar Energy*, *82*(11), 977–985. https://doi.org/10.1016/j.solener.2008.05.006

Kahwaji, S., Johnson, M. B., Kheirabadi, A. C., Groulx, D., & White, M. A. (2018). A comprehensive study of properties of paraffin phase change materials for solar thermal energy storage and thermal management applications. *Energy*, *162*, 1169–1182. https://doi.org/10.1016/j.energy.2018.08.068

Klimeš, L., Charvát, P., Mastani Joybari, M., Zálešák, M., Haghighat, F., Panchabikesan, K., El Mankibi, M., & Yuan, Y. (2020). Computer modelling and experimental investigation of phase change hysteresis of PCMs: The state-of-the-art review. *Applied Energy*, *263*(August 2019), 114572. https://doi.org/10.1016/j.apenergy.2020.114572

König-Haagen, A., Faden, M., & Diarce, G. (2023). A CFD results-based reduced-order model for latent heat thermal energy storage systems with macro-encapsulated PCM. *Journal of Energy Storage*, *73*(May). https://doi.org/10.1016/j.est.2023.109235

Madruga, S., Haruki, N., & Horibe, A. (2018). Experimental and numerical study of melting of the phase change material tetracosane. *International Communications in Heat and Mass Transfer*, *98*(September), 163–170. https://doi.org/10.1016/j.icheatmasstransfer.2018.08.021

Momeni, M., Jalilian, S., & Fartaj, A. (2023). Heat Transfer Analysis of a Crossflow Minichannel Heat Exchanger Based on Air and Liquid Flow. *International Conference on Fluid Flow, Heat and Mass Transfer*, *10*, 86–96. https://doi.org/10.11159/ffhmt23.110

Neumann, H., Gamisch, S., & Gschwander, S. (2021). Comparison of RC-model and FEM-model for a PCM-plate storage including free convection. *Applied Thermal Engineering*, *196*(September 2020), 117232. https://doi.org/10.1016/j.applthermaleng.2021.117232

Piroozmand, V., & Ahmadi, R. (2024). Enhancement of PCMs performance using nano-particles in horizontal triple-series shell-and-tube heat exchangers: A numerical study. *Journal of Energy Storage*, *85*(December 2023), 111057. https://doi.org/10.1016/j.est.2024.111057

Rubitherm GmbH. (2024a). Rubitherm GmbH. In *RUBITHERM RT55 Phase change material*. http://rubitherm.de/%0Ahttp://www.rubitherm.eu/

Rubitherm GmbH. (2024b). Rubitherm GmbH. *RUBITHERM RT62HC Phase Change Material*.

Zhang, Y., Bozorg, M. V., Torres, J. F., Zhao, Y., & Wang, X. (2022). Dynamic melting of encapsulated PCM in various geometries driven by natural convection of surrounding air: A modelling-based parametric study. *Journal of Energy Storage*, *48*(January), 103975. https://doi.org/10.1016/j.est.2022.103975

Zheng, H., Wang, C., Liu, Q., Tian, Z., & Fan, X. (2018). Thermal performance of copper foam/paraffin composite phase change material. *Energy Conversion and Management*, *157*(September 2017), 372–381. https://doi.org/10.1016/j.enconman.2017.12.023

ACKNOWLEDGEMENT

This material is based upon work supported by the U.S. Department of Energy's Office of Energy Efficiency and Renewable Energy (EERE) under the Building Technologies Office (BTO) Award Number DE-EE0009158. The views expressed herein do not necessarily represent the views of the U.S. Department of Energy or the United States Government. This work was also supported in part by the Modeling & Optimization Consortium at the Center for Environmental Energy Engineering at the University of Maryland.